JACS
JOURNAL OF THE AMERICAN CHEMICAL SOCIETY

Communication

pubs.acs.org/JACS

Enhancing Visible Light Photo-oxidation of Water with TiO_2 Nanowire Arrays via Cotreatment with H_2 and NH_3: Synergistic Effects between Ti^{3+} and N

Son Hoang, Sean P. Berglund, Nathan T. Hahn, Allen J. Bard, and C. Buddie Mullins*

Departments of Chemical Engineering and Chemistry and Biochemistry, Center for Electrochemistry, Texas Materials Institute, Center for Nano- and Molecular Science, University of Texas at Austin, 1 University Station C0400, Austin, Texas 78712-0231, United States

Supporting Information

ABSTRACT: We report a synergistic effect involving hydrogenation and nitridation cotreatment of TiO_2 nanowire (NW) arrays that improves the water photo-oxidation performance under visible light illumination. The visible light (>420 nm) photocurrent of the cotreated TiO_2 is 0.16 mA/cm^2 and accounts for 41% of the total photocurrent under simulated AM 1.5 G illumination. Electron paramagnetic resonance (EPR) spectroscopy reveals that the concentration of Ti^{3+} species in the bulk of the TiO_2 following hydrogenation and nitridation cotreatment is significantly higher than that of the sample treated solely with ammonia. It is believed that the interaction between the N-dopant and Ti^{3+} is the key to the extension of the active spectrum and the superior visible light water photo-oxidation activity of the hydrogenation and nitridation cotreated TiO_2 NW arrays.

The search for cheap, efficient, and stable photocatalysts for solar hydrogen production from water splitting has been an increasingly active field since Honda and Fujishima's discovery of water photo-oxidation on a TiO_2 photoanode under ultraviolet (UV) light.[1] To date, TiO_2 is still one of the most studied photocatalyst materials due to its abundance, low cost, low toxicity, superior photostability, and high intrinsic catalytic activity under UV illumination.[2−5] However, the photoconversion efficiency of TiO_2 is limited to less than 2.2% under AM 1.5 global solar illumination due to its large band gap energy (3.0 eV for rutile and 3.2 eV for anatase).[6] The generally accepted benchmark for solar-to-hydrogen efficiency under AM 1.5 global illumination is 10% for practical implementation.[7] Therefore, extending the working spectrum of TiO_2-based materials to include more of the visible light region, which composes ∼45% of the total energy of the solar spectrum, has been of great interest.

Recent efforts have focused on modifying the valence band of TiO_2 by incorporating nonmetal ions such as C,[8] S,[9] and N.[4,10] The p states of the nonmetal foreign ions (N, S, or C) normally form impurity states above the valence band or hybridize with O 2p states (composing most of the valence band for TiO_2) thus upshifting the valence band edge of TiO_2.[3] Among nonmetal elements, N doping has been widely investigated and some success has been achieved in extending the working spectrum of TiO_2 toward the visible light range.[4] Modifying TiO_2 by hydrogen has also received attention recently.[11,12] Wang et al. demonstrated that annealing rutile TiO_2 nanowire (NW) arrays in a H_2 atmosphere creates oxygen vacancy sites thus forming donor states below the conduction band.[11] This improves light absorption and charge transport similar to n-type doping, thus enhancing water oxidation performance. Chen et al. reported a hydrogenation method to produce disorder in nanophase TiO_2, which significantly enhances visible light absorption.[12] Despite the interest in the effects of nitrogen doping and hydrogen modification, there are only a few studies on the synergistic effects of H and N codoping on the photocatalytic activity of TiO_2 materials.[13−17] To our knowledge, there is no report on the enhancement of visible light water photo-oxidation of TiO_2 due to the cotreatment with H_2 and NH_3 at high temperature. Diwald et al. prepared H, N-codoped TiO_2 material that is photoactive for Ag deposition under irradiation by photons of 2.4 eV by annealing rutile TiO_2 (110) in NH_3 at 870 K. The treatment introduced two species of N into the TiO_2 lattice: substitutional and interstitial N species.[17] The authors claimed that the codoping effect between the interstitial species and hydrogen is responsible for the enhancement in the visible light activity. The authors, however, did not consider the effects of Ti^{3+} formation. In fact, under this nitridation condition, Ti^{3+} formation is expected and can be more readily detected using bulk characterization techniques such as EPR rather than by conventional surface characterization techniques such as X-ray Photoemission Spectroscopy (XPS) due to the instability of the surface Ti^{3+} in air or water.

In addition to enhancing optical absorption, it is equally important to optimize the photogenerated electron/hole separation characteristics. Vertically oriented nanocolumnar structures are considered to be very effective structures for photoelectrochemical (PEC) water splitting applications.[18,19] These structures permit significant light absorption depths while still enhancing the charge separation by providing high electrode/electrolyte interface areas and shortening the minority charge carrier transport distance to the electrolyte. We have recently reported the hydrothermal synthesis of vertically aligned ultrafine single crystalline rutile TiO_2 NW arrays with an average cross-sectional dimension of ∼5 nm.[10]

Received: December 5, 2011
Published: February 8, 2012

dx.doi.org/10.1021/ja211369s | J. Am. Chem. Soc. 2012, 134, 3659−3662

Upon nitridation in a NH_3 flow at 500 °C, the optical absorption and the PEC response spectrum extended from ~420 to ~550 nm. In the present study, we demonstrate synergistic effects of hydrogenation and nitridation that further extend the active spectrum of the TiO_2 NW arrays to ~570 nm. To our knowledge, we are the first to demonstrate the enhancement of visible light water photo-oxidation reactivity of TiO_2 material due to hydrogenation and nitridation cotreatment.

The TiO_2 photoelectrodes were prepared via two steps: (1) hydrothermal synthesis followed by (2) thermal treatments. The single crystalline rutile TiO_2 NW arrays with a thickness of 2.60 ± 0.27 μm were hydrothermally prepared on Fluorine-doped Tin Oxide (FTO) substrates. The NW arrays were further modified by annealing at 500 °C (i) in air for 1 h (denoted as TiO_2), (ii) in NH_3 for 2 h (N-TiO_2), (iii) in a mixture of H_2 and Ar (5% of H_2) for 1 h (H-TiO_2), and (iv) in a mixture of H_2 and Ar for 1 h followed by annealing in NH_3 for 2 h (H, N-TiO_2). Additional experimental details on the hydrothermal synthesis and thermal treatments can be found in the Supporting Information (SI).

The X-ray diffraction data (XRD) (SI, Figure S2a) confirm that all films are of rutile phase and no additional phase was detected upon thermal treatment. However, the thermal treatments have a profound effect on the visual appearance and morphology of the NW arrays. The white color of the pristine TiO_2 film did not change after hydrogen treatment; however, it turned green after nitridation and dark green after both treatments (SI, Figure S1). In addition the shape and size of the nanowires changed with each treatment as can be seen by the SEM images in Figure 1. Upon treatment, the cross

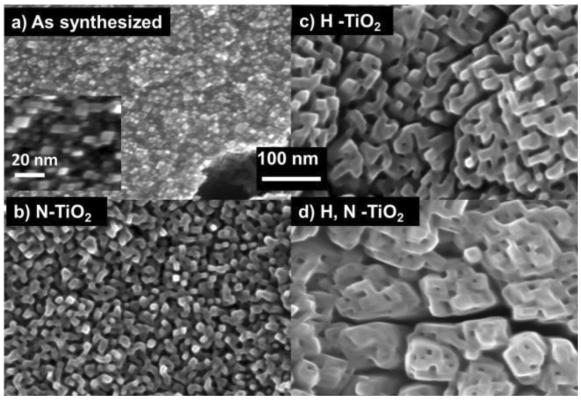

Figure 1. Scanning Electron Microscopy (SEM) images of (a) as-synthesized TiO_2 (inset shows higher magnification view), and films annealed at 500 °C in (b) NH_3, (c) H_2, and (d) H_2 and then NH_3.

section of the NW becomes larger due to the sintering of the small wires. Increases in the interplanar *d*-spacing for the (101) crystal plane due to cotreatment observed by Transmission Electron Microscopy (TEM) (SI, Figure S3) indicate lattice expansion as a result of N incorporation.

We employed X-ray Photoemission Spectroscopy (XPS) to investigate the chemical composition of the surface (Figure 2). The N 1s peak at 399.8 eV of the TiO_2 sample is assigned to molecular N_2 adsorbed on the surface.[4] The N 1s feature at 395.6 eV of the N-TiO_2 sample and the feature at 394.4 eV of the H, N-TiO_2 sample are assigned to substitutional β-N (N^{3-}) species which is considered responsible for enhancing the visible light activity of the N-doped materials.[4,20] It is

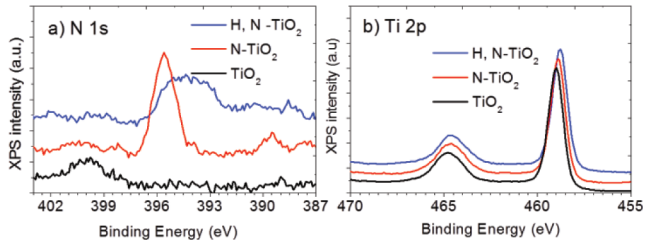

Figure 2. XPS spectra of the TiO_2, N-TiO_2, and H, N-TiO_2 NW arrays: (a) Core N 1s and (b) Core Ti 2p.

interesting that the N 1s feature of the H, N-TiO_2 sample is broader and shifts to a lower binding energy compared with that of the N-TiO_2. We will discuss these phenomena in more detail later. The substitutional N concentrations are calculated as 5.6 atomic % for N-TiO_2 and 3.5 atomic % for H, N-TiO_2, corresponding to x values of 0.20 and 0.12 (x in $TiO_{2-x}N_x$), respectively. The substitutional N concentration in our N-modified TiO_2 nanowires is considerably higher compared to other N-doped TiO_2 materials prepared via nitridation of TiO_2 at elevated temperature in a NH_3 flow.[21] The unique morphology and the ultrafine cross-section of the NW may enhance N diffusion into the TiO_2 lattice.

The Ti 2p3/2 XPS features are observed at 459.20, 458.76, and 458.71 eV for TiO_2, N-TiO_2, and H, N-TiO_2 respectively. These features are all assigned to Ti^{4+}, indicating no Ti^{3+} species exist on the surface (the XPS technique characterizes the top 1−10 nm layer of the material). The presence of Ti^{3+} was further investigated by low temperature electron paramagnetic resonance (EPR) (Figure 3). No EPR features appear

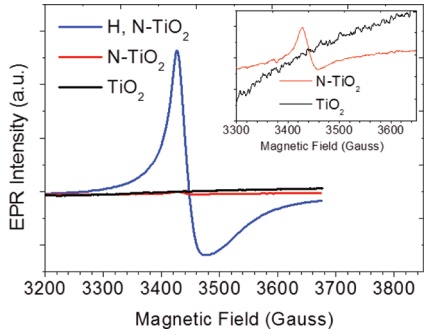

Figure 3. EPR spectra recorded at 86 K for TiO_2, N-TiO_2, and H, N-TiO_2 samples. The inset shows magnified view for the EPR spectra of the TiO_2 and N-TiO_2 samples.

for a *g*-value of ~2.02 corresponding to O_2^- produced from the reduction of adsorbed O_2 (from air) by surface Ti^{3+} further confirming the absence of surface Ti^{3+}.[22] Surface Ti^{3+} is unstable under illumination in air or in electrolyte as it is easily oxidized by air or dissolved oxygen in water.[23] The strong EPR signal for a *g*-value of 1.992 for the H, N-TiO_2 sample indicates the presence of Ti^{3+} in the bulk. We also observed a trace amount of Ti^{3+} in the bulk of the N-TiO_2 sample. The intensity of the feature at a g-value of 1.981 for the N-TiO_2 sample is 2 orders of magnitude smaller than the feature at a *g*-value of 1.992 for the H, N-TiO_2 sample.

Linear sweep voltammetry (scan rate of 5 mV/s) results for the H, N-TiO_2 nanowires are shown in Figure 4a. The onset potential for the H, N-TiO_2 sample positively shifts to 0.6 V vs reversible hydrogen electrode (V_{RHE}) compared with 0.2 V_{RHE}

dx.doi.org/10.1021/ja211369s | J. Am. Chem. Soc. 2012, 134, 3659−3662

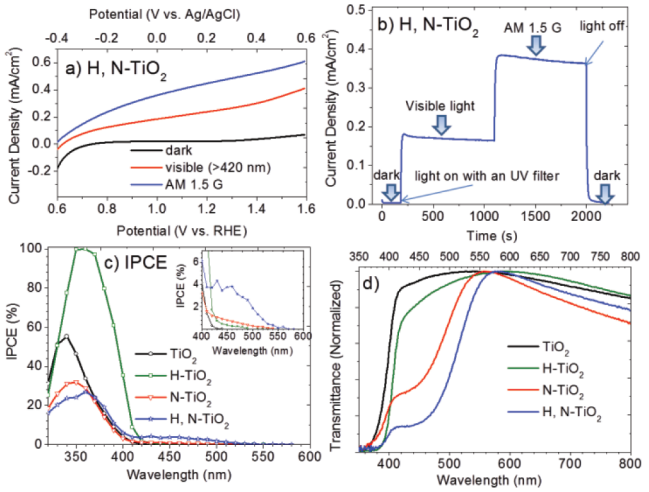

Figure 4. (a and b) Linear sweep voltametry (5 mV/s) and chronoamperometry at 1.23 V_{RHE} of the H, N-TiO_2 sample, (c) IPCE spectra measured at 1.23 V_{RHE}, and (d) normalized transmittance spectra. All PEC measurements were performed using a three-electrode electrochemical cell with a Ag/AgCl reference electrode, a Pt wire counter electrode, and 1 M KOH electrolyte. A solar simulator (Oriel 96000) with an AM 1.5 G filter was used as the light source with a light intensity of 100 mW/cm^2 measured by a thermopile detector (Newport, 818P-020-12). A UV filter that blocks all wavelengths <420 nm was used for visible light experiments.

for the pristine TiO_2 sample even though the photocurrent transient onset potentials for the two sample are almost the same, ~ −0.15 V_{RHE} (data not shown). The shift in the constant-illumination onset potential might be due to either a larger band bending requirement for separating electrons and holes because of the material's likely possession of poorer charge-transport properties than pure TiO_2 or slower surface kinetics as a result of hydrogenation and nitridation cotreatment.[10] The H, N-TiO_2 sample shows remarkable visible light water oxidation performance. The visible light (>420 nm) current reaches 0.159 mA/cm^2 at 1.23 V vs reversible hydrogen electrode (V_{RHE}) and contributes ~41% of the full AM 1.5 G photocurrent. The chronoamperometry (CAM) measurement at 1.23 V_{RHE} (total time of ~30 min) in Figure 4b indicates the material's high stability. After the test, we observed the formation of bubbles on the film, suggesting the oxygen production from water oxidation. We believe that the formation of oxygen bubbles decreases the electrode/electrolyte contact area, resulting in a slight decrease of 4.6% in the AM 1.5 G photocurrent after 15 min of illumination. Figure S4 shows 3 runs of CAM measurements between which we used a pipet to flush out bubbles on the sample. The photocurrents were almost fully restored, thus supporting our hypothesis. In fact, after repeated testing for 5 months (the sample was stored in open air) the film still retains this performance. Figure 4c and d show the incident photon-to-current efficiency (IPCE) spectra and the normalized UV−vis transmittance spectra (the raw data are included in the SI, Figure S5). The absorption edge of the H, N-TiO_2 sample shifts ~20 nm to the longer wavelength region compared to the N-doped TiO_2 NW sample. The decrease in the transmittance for all samples at larger wavelengths than 570 nm is due to the light absorption of FTO substrates in this region which is confirmed by the UV−vis transmittance of FTO in Figure S5. The IPCE spectra fit well with the transmittance spectra, confirming that the active spectra of the H, N-TiO_2 sample extends to ~570 nm. The photocurrent obtained by integrating the calculated IPCE multiplied by the AM 1.5 G solar energy flux[24] over the range of 420−570 nm is 0.159 mA/cm^2, contributing to ~35% of the total integrated AM 1.5 G photocurrent (0.454 mA/cm^2). The small discrepancy between the full AM 1.5 G photocurrent obtained by the CAM measurement (0.388 mA/cm^2) and the integration method (0.454 mA/cm^2) might be due to the difference between the simulated sunlight (Xenon lamp + AM 1.5 G filter) and standard AM 1.5 G. The absence of a photoresponse in the IPCE of the untreated TiO_2 NW arrays indicates that the absorption tails from 420 to 500 nm in the transmittance spectra of the untreated TiO_2 sample are due to light scattering from the nanostructures. The H-TiO_2 sample shows significant improvement in the PEC performance in the UV region due to the enhancement in the electron conductivity.[11] Its IPCE spectrum, however, just shows a weak response from visible light (420 to ~500 nm), mainly due to the photoelectrochemically inactive transition from the valence band to hydrogenation-induced oxygen vacancy states.[11]

As mentioned in our previous study, incorporating N into the rutile TiO_2 NW arrays modifies the valence band structure, thus extending the working spectrum to ~550 nm. In the present study, we demonstrate that prehydrogenation significantly increases the bulk Ti^{3+} concentration and the interaction between Ti^{3+} and N-doping increases the visible light absorption and shifts the absorption edge further to the longer wavelength region (~ 570 nm) compared to individual doping with Ti^{3+} or N. Employing EPR, Livraghi et al. detected paramagnetic bulk species of N ($N_b^{\cdot}$) at a g-value of 2.005, which formed localized states within the band gap of their N-doped TiO_2.[25] The authors proposed a reversible electron transfer between the $N_b^{\cdot}$ and Ti^{3+} centers forming the diamagnectic bulk species of N (N_b^-) and Ti^{4+}. A similar phenomenon was also observed by Napoli et al. when they exposed a prereduced TiO_2 to a N plasma.[26] The N-induced states of N_b^- species are higher in energy than that of corresponding N_b species due to greater Coulombic repulsion. Di Valentin et al. prepared F, N-codoped TiO_2 samples and reported an increase in Ti^{3+} concentration with an increasing F doping level. The authors also claimed that the formation of N_b^- is more favorable with an increase in Ti^{3+} and that is the key for the improvement in the visible light photocatalytic activity.[27] We did not detect any paramagnetic species other than Ti^{3+} in our H, N-TiO_2 sample. We, however, can observe the interactions of Ti^{3+} and substitutional N in the H, N-TiO_2 sample in the core N 1s XPS spectra (Figure 2a). The broadening and shift to the lower binding energy of the XPS N 1s feature compared with that of the N-TiO_2 sample indicates lower oxidation states of the substitutional N in the H, N-TiO_2 sample which might be due to electron transfer from Ti^{3+}. Due to the Columbic repulsion, the lower oxidation states of N in the H, N-TiO_2 sample have higher energy than that of the N-TiO_2 sample, thus enabling excitation with photons of longer wavelengths. The proposed interaction between Ti^{3+} and N that modifies the electronic band structure of TiO_2 is illustrated in Figure 5.

In summary, we report a synergistic effect between hydrogen and nitridation cotreatment that significantly enhances the water photo-oxidation of rutile TiO_2 NW arrays under visible light. The photocurrent of the H, N-TiO_2 sample under visible light (>420 nm) illumination contributes ~41% of the

dx.doi.org/10.1021/ja211369s | J. Am. Chem. Soc. 2012, 134, 3659−3662

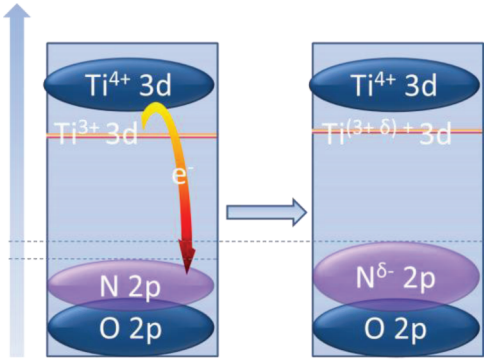

Figure 5. Proposed mechanism for the interaction between Ti^{3+} and substitutional N.

simulated AM 1.5 G photocurrent. The IPCE and UV−vis transmittance spectroscopy reveal that the working spectrum of the H, N-TiO_2 sample extends to ∼570 nm compared with ∼550 nm for the N-TiO_2 and ∼420 nm for pristine TiO_2. The hydrogenation process increases the bulk Ti^{3+} concentration in TiO_2. We speculate that the interactions between substitutional N and Ti^{3+} are responsible for the enhancement in the water oxidation performance under visible light illumination.

■ ASSOCIATED CONTENT

Supporting Information

Full experimental details, digital images, XPS, XRD, TEM, raw data of UV−vis transmittance, and the incident power density used in the IPCE measurements. This material is available free of charge via the Internet at http://pubs.acs.org.

■ AUTHOR INFORMATION

Corresponding Author

mullins@che.utexas.edu

Notes

The authors declare no competing financial interest.

■ ACKNOWLEDGMENTS

The authors gratefully acknowledge (i) the Division of Chemical Sciences, Geosciences, and Biosciences, Office of Basic Energy Sciences of the U.S. Department of Energy through Grant DE-FG02-09ER16119 and (ii) the Welch Foundation (C.B.M. for Grant F-1436 and A.J.B. for Grant F-0021). We would like to thank Minh Nguyen for help with EPR measurements and Vince Holmberg and Professor Brian Korgel for help with the UV−vis transmittance measurements.

■ REFERENCES

(1) Fujishima, A.; Honda, K. *Nature* **1972**, *238*, 37−38.
(2) Linsebigler, A. L.; Lu, G.; Yates, J. T. *Chem. Rev.* **1995**, *95*, 735−758.
(3) Chen, X.; Mao, S. S. *Chem. Rev.* **2007**, *107*, 2891−2959.
(4) Asahi, R.; Morikawa, T.; Ohwaki, T.; Aoki, K.; Taga, Y. *Science* **2001**, *293*, 269−271.
(5) Leary, R.; Westwood, A. *Carbon* **2011**, *49*, 741−772.
(6) Murphy, A. B.; Barnes, P. R. F.; Randeniya, L. K.; Plumb, I. C.; Grey, I. E.; Horne, M. D.; Glasscock, J. A. *Int. J. Hydrogen Energy* **2006**, *31*, 1999−2017.
(7) Bard, A. J.; Fox, M. A. *Acc. Chem. Res.* **1995**, *28*, 141−145.
(8) Park, J. H.; Kim, S.; Bard, A. J. *Nano Lett.* **2006**, *6*, 24−28.
(9) Umebayashi, T.; Yamaki, T.; Itoh, H.; Asai, K. *Appl. Phys. Lett.* **2002**, *81*, 454−456.
(10) Hoang, S.; Guo, S.; Hahn, N. T.; Bard, A. J.; Mullins, C. B. *Nano Lett.* **2012**, *12*, 26−32.
(11) Wang, G.; Wang, H.; Ling, Y.; Tang, Y.; Yang, X.; Fitzmorris, R. C.; Wang, C.; Zhang, J. Z.; Li, Y. *Nano Lett.* **2011**, *11*, 3026−3033.
(12) Chen, X.; Liu, L.; Yu, P. Y.; Mao, S. S. *Science* **2011**, *331*, 746−750.
(13) Mi, L.; Zhang, Y.; Wang, P. N. *Chem. Phys. Lett.* **2008**, *458*, 341−345.
(14) Russo, S. P.; Grey, I. E.; Wilson, N. C. *J. Phys. Chem. C* **2008**, *112*, 7653−7664.
(15) Pan, H.; Zhang, Y.-W.; Shenoy, V. B.; Gao, H. *J. Phys. Chem. C* **2011**, *115*, 12224−12231.
(16) Lan, M.; Peng, X.; Hong, S.; Pei-Nan, W.; Weidian, S. *Appl. Phys. Lett.* **2007**, *90*, 171909.
(17) Diwald, O.; Thompson, T. L.; Zubkov, T.; Walck, S. D.; Yates, J. T. *J. Phys. Chem. B* **2004**, *108*, 6004−6008.
(18) Hahn, N. T.; Ye, H.; Flaherty, D. W.; Bard, A. J.; Mullins, C. B. *ACS Nano* **2010**, *4*, 1977−1986.
(19) van de Krol, R.; Liang, Y. Q.; Schoonman, J. *J. Mater. Chem.* **2008**, *18*, 2311−2320.
(20) Takahashi, I.; Payne, D. J.; Palgrave, R. G.; Egdell, R. G. *Chem. Phys. Lett.* **2008**, *454*, 314−317.
(21) Wang, J.; Tafen, D. N.; Lewis, J. P.; Hong, Z.; Manivannan, A.; Zhi, M.; Li, M.; Wu, N. *J. Am. Chem. Soc.* **2009**, *131*, 12290−12297.
(22) Anpo, M.; Che, M.; Fubini, B.; Garrone, E.; Giamello, E.; Paganini, M. *Top. Catal.* **1999**, *8*, 189−198.
(23) Teleki, A.; Pratsinis, S. E. *Phys. Chem. Chem. Phys.* **2009**, *11*, 3742−3747.
(24) http://rredc.nrel.gov/solar/spectra/am1.5/.
(25) Livraghi, S.; Paganini, M. C.; Giamello, E.; Selloni, A.; Di Valentin, C.; Pacchioni, G. *J. Am. Chem. Soc.* **2006**, *128*, 15666−15671.
(26) Napoli, F.; Chiesa, M.; Livraghi, S.; Giamello, E.; Agnoli, S.; Granozzi, G.; Pacchioni, G.; Di Valentin, C. *Chem. Phys. Lett.* **2009**, *477*, 135−138.
(27) Di Valentin, C.; Finazzi, E.; Pacchioni, G.; Selloni, A.; Livraghi, S.; Czoska, A. M.; Paganini, M. C.; Giamello, E. *Chem. Mater.* **2008**, *20*, 3706−3714.